Natural Domain Design: Enhanced Thermal Stability of a Zinc-Lacking Ferredoxin Isoform Shows that a Hydrophobic Core Efficiently Replaces the Structural Metal Site†

Rita Rocha,‡ Sónia S. Leal,‡ Vitor H. Teixeira,‡ Manuela Regalla,‡ Harald Huber,§ António M. Baptista,‡ Cláudio M. Soares,‡ and Cláudio M. Gomes*,‡

Instituto Tecnologia Química e Biológica, Universidade Nova de Lisboa, Oeiras, Portugal, and Lehrstuhl fuer Mikrobiologie der Universitaet Regensburg, 93053 Regensburg, Germany

Received May 30, 2006; Revised Manuscript Received June 29, 2006

ABSTRACT: Zinc centers play a key role as important structure determinants in a variety of proteins including ferredoxins (Fd). Here, we exploit the availability of two highly similar ferredoxin isoforms from the thermophile *Sulfolobus metallicus*, which differ in the residues involved in coordinating a His/Asp zinc site that ties together the protein core with its *N*-terminal extension, to investigate the effect of the absence of this site on ferredoxin folding. The conformational properties of the zinc-containing (FdA) and zinc-lacking (FdB) isoforms were investigated using visible absorption and tryptophan fluorescence emission. Fluorescence quenching studies, together with comparative modeling and molecular dynamics simulations, indicate that the FdB *N*-terminal extension assumes a fold identical to that of the Zn^{2+}-containing isoform. The thermal stability of the isoforms was investigated in a broad pH range ($2 < pH < 10$), and at physiological pH conditions, both proteins unfold above 100 °C. Surprisingly, the Zn^{2+}-lacking isoform was always found to be more stable than its Zn^{2+}-containing counterpart: a $\Delta T_m \approx 9$ °C is determined at pH 7, a difference that becomes even more significant at extreme pH values, reaching a $\Delta T_m \approx 24$ °C at pH 2 and 10. The contribution of the Zn^{2+} site to ferredoxin stability was further resolved using selective metal chelators. During thermal unfolding, the zinc scavenger TPEN significantly lowers the T_m in FdA (≈10 °C), whereas it has no effect in FdB. This shows that the Zn^{2+} site contributes to ferredoxin stability but that FdB has devised a structural strategy that accounts for an enhanced stability without using a metal cross-linker. An analysis of the FdB sequence and structural model leads us to propose that the higher stability of the zinc-containing ferredoxin results from van der Waals contacts formed between the residues that occupy the same spatial region where the zinc ligands are found in FdA. These favor the formation of a novel local stabilizing hydrophobic core and illustrate a strategy of natural fold design.

The tertiary structure of a protein is mainly stabilized by weak noncovalent interactions that have an additive effect toward fold stabilization. Salt bridges (12.5−17 kJ·mol^{-1}), hydrogen bonds (2−6 kJ·mol^{-1}), and van der Waals interactions (4−17 kJ·mol^{-1}) present within a protein contribute to a net stabilizing effect toward the folded structure, which is nevertheless only marginally stable in water at physiological temperature ($\Delta G_U \approx 20-40$ kJ·mol^{-1}) (*1*). However, the topological arrangement of secondary structure elements in a particular local motif can also involve additional covalent interactions that act as natural cross-linkers of a particular conformation. The most common protein covalent modifications are disulfide bridges (167 kJ·mol^{-1}) that involve the oxidation of two sulfhydryl groups from nearby cysteine residues, which can also have a functional role (*2*).

Another common cross-linking interaction in proteins is the one involving the formation of coordinate covalent bonds between a metal ion and protein ligands. These structural metal sites, which provide stabilization at a particular region of a protein, are most frequently occupied by calcium (Ca^{2+}) and zinc (Zn^{2+}) ions (*1*). The latter are typified by the so-called zinc-finger motifs (*3*, *4*), in which various combinations of four cysteine or histidine residues in a short sequence stretch of around 30 residues bind a Zn^{2+} ion that stabilizes a local domain comprising an α-helix and three β-strands (*3*). This is the most abundant structural domain in the human genome, and in the absence of the metal, it unfolds (*5*). There are a plethora of examples in which the engineering of a zinc site in a protein results in an important increase in its thermodynamic stability. For example, adenylate kinases (AK) from gram-positive bacteria hold a structural Zn^{2+} site, whereas those from gram-negative bacteria lack it. Site directed mutagenesis in the AK from gram-negative *Escherichia coli* introducing a zinc site results in a protein with an increased thermal stability ($\Delta T_m = 9$ °C) (*6*, *7*). There

† This work was supported by research grants POCTI/QUI/37521 and POCTI/QUI/45758 (to C.M.G.) from the Fundação Ciência e Tecnologia (FCT/MCES, Portugal). S.S.L. and V.H.T. are recipients of Ph.D. fellowships from Fundação para a Ciência e Tecnologia (references SFRH/BD/18653/2004 and SFRH/BD/6477/2001, respectively).

* To whom correspondence should be addressed. Tel: +351 214469332. Fax: +351 214411277. E-mail: gomes@itqb.unl.pt.

‡ Universidade Nova de Lisboa.

§ Universitaet Regensburg.

10.1021/bi0610698 CCC: $33.50
Published on Web 08/03/2006

are also several examples of Zn-containing proteins in which metal removal results in decreased stability (*8*, *9*).

Zinc structural sites encompass a versatile combination of soft (Cys, His) and hard (Asp, Glu) ligands, a feature also denoted in some catalytic zinc centers (*3*, *10*). In fact, protein coordination in structural zinc sites is diverse and ranges from the preferred all cysteine coordination to sites in which Asp and Glu are found in combination with His residues. Such a His/Asp site has also been identified in ferredoxins (*11*, *12*) isolated from organisms belonging to the Archaeal order of the Sulfolobales. These proteins are structurally characterized by having two Fe−S clusters (a [3Fe4S] and a [4Fe4S]) and a 36 amino acid long *N*-terminal extension comprising three β-strands. This part of the protein comprises the three His residues that bind Zn^{2+}, whereas the Asp comes from the protein core, completing a tetrahedral coordination. Thus, this zinc center has been suggested to play an important role in stabilizing the protein structure. In fact, the mutagenesis of any of its His ligands results in a destabilized protein (*13*, *14*). Interestingly, some ferredoxins from this family were found to naturally lack the zinc site, and in some instances, both zinc-containing and -lacking isoforms are simultaneously expressed (*12*).

We have a long standing interest in the characterization of the biochemical, structural and stability properties of Fe−S proteins (*12*, *15*−*17*), and at this point, we turned our attention toward the two ferredoxin isoforms available from *Sulfolobus metallicus*, with and without the Zn^{2+} center. The rationale of our approach was to investigate the effect of zinc site removal on the protein fold by determining the stability differences between the two ferredoxin isoforms, which have a very high percentage of amino acid identity (>80%) throughout most of their sequences, but differ precisely in the residues involved in coordinating the zinc site that ties together the protein core with its *N*-terminal extension. The results obtained in this work were a surprise with respect to initial expectations: the zinc-lacking ferredoxin isoform is not destabilized by the absence of the center, but in fact, it has an enhanced stability with respect to the zinc-containing protein. These findings illustrate a natural fold design strategy because during evolution, nature has found multiple alternative strategies within the same protein family to achieve stabilization of a particular fold. This leads to the proposal that the higher stability of the zinc-containing ferredoxin results from novel nonpolar interactions present in the same spatial region where the zinc center is found in the other isoforms, which favor the formation of a local stabilizing hydrophobic core.

EXPERIMENTAL PROCEDURES

Chemicals. All reagents were of the highest purity grade commercially available. The chemical denaturant Guanidinium hydrochloride (GuHCl) was obtained from Promega, and the accurate concentration of the stock solutions in different buffers was confirmed by refractive index measurements. The chelator ethylenediaminetetraacetic acid (EDTA[1]) was purchased from Merck. The chelators desferrioxamine (DFO) and *N*,*N*,*N*′,*N*′-tetrakis(2-pyridylmethyl) ethylenediamine (TPEN) were from Sigma.

Protein Purification. The ferredoxins from *Sulfolobus metallicus* used in this work were purified as previously described (*12*). Briefly, after cell disruption in 40 mM potassium phosphate at pH 6.5 (buffer A), the resulting cytosolic fraction was applied to a Q-sepharose fast flow column ($V_c = 20$ mL), and the Fd-containing fractions eluted at ∼200−350 mM NaCl. After concentration in 5 kDa amicons, this fraction was loaded onto a Superdex G-50 column ($V_c = 150$ mL), eluted with buffer A + 150 mM NaCl, and pooled according to the typical visible spectra of Fds. This fraction containing a mixture of FdA and FdB was dialyzed against buffer A and further resolved in a high performance Q-sepharose column ($V_c = 20$ mL), after application of a flat salt gradient from which two separated peaks were obtained. Protein purity was confirmed by SDS−PAGE and *N*-terminus sequencing, and the stocks were kept as concentrated aliquots at −20 °C.

Protein Sequencing. The ferredoxin sequencing procedures were identical to those previously described for the *Acidianus* ambivalens ferredoxin (*12*), with some minor modifications. For complete sequence determination, ∼100 μg of FdA and FdB were carboxymethylated following published procedures (*18*). The resulting samples were divided into three aliquots, which were processed in three distinct steps. Two of the steps were common for FdA and FdB and consisted of *N*-terminal sequencing and chemical cleavage. The chemical cleavage with CNBr was carried out by adding a CNBr crystal to the carboxymethylated polypeptides dissolved in 70% of formic acid. After an incubation period of 24 h in the dark, the reagents were evaporated and the resulting peptides resuspended. The third step consisted of an enzymatic digestion step using endoproteinases and was different for the two proteins: FdA was subjected to specific hydrolysis by Asp-N (Roche Diagnostics GmbH), whereas FdB was digested with Asp-N and Lys-C (Roche Diagnostics GmbH). Digestions were carried out following the manufacturer's instructions, typically for 18 h and with a 1:100 enzyme to polypeptide mass ratio. The peptide fragments produced in each of the cleavage steps were separated by reverse-phase HPLC on a Beckmann Gold System using a 3.9 × 150 mm C_{18} column (Delta-Pak 300A, Waters), a gradient of 0−80% acetonitrile in 0.1% aqueous TFA as the eluent and a flow rate of 0.5 mL min^{-1}. The peptide bands were detected in the effluent by UV absorption at 214 nm and sequenced. These sequences together with the *N*-terminal sequence (up to residue ∼50) were used to build a peptide map from which the ferredoxin sequences were inferred. Sequencing was carried out on an Applied Biosystems Procise 491 HT sequencer.

Spectroscopic and Biochemical Methods. UV−vis spectra were recorded using a Shimadzu Multispec-1501 diode array spectrophotometer equipped with cell stirring and temperature control by a Julabo 4 MV water bath. Fluorescence spectroscopy was performed using a Cary Varian Eclipse instrument equipped with cell stirring and a Peltier temperature control. Protein concentrations were determined by using either the method of Bradford or the extinction coefficient ($\epsilon^{410\ nm} = 30.4\ mM^{-1}\ cm^{-1}$). For pH variations, the buffers (20 mM) used were acetate (pH 4), HEPES, or potassium phosphate (pH ∼7) and glycine (pH 2 and 10); the effect of the variation of the pH with temperature was

[1] Abbreviations: Fd, ferredoxin; RMSD, root-mean-square deviation; MD, molecular dynamics; TPEN, *N*,*N*,*N*′,*N*′-tetrakis(2-pyridylmethyl) ethylenediamine; EDTA, ethylenediamine tetra acetic acid; DFO, desferrioxamine.

verified or taken into consideration in buffer preparation. Metal analysis (iron and zinc) was carried out by total reflection X-ray fluorescence (TXRF) at the laboratory of Professor B. O. Kolbesen at the Inst. für Anorg. und Analyt. Chemie (Johann Wolfgang Goethe-Universität, Frankfurt, Germany).

Comparative Modeling. Comparative modeling was carried out using two structures as structural templates: the ferredoxin from *Sulfolobus tokodaii* (*11*) (pdb: 1xer) and that from *Acidianus ambivalens* (Frazão et al., personal communication), both determined at 2 Å resolution. While the former had the merit of eliciting the presence of a Zn site, it lacked density around the [4Fe4S] site region, thus preventing a detailed description of an important part of the protein core structure. This limitation is circumvented with the use of the *A. ambivalens* ferredoxin structure, which provides a complete description of the Fe−S moieties. Some residues of the *Aa*FdA had alternative conformations, and for those, the one with the largest occupation value was chosen. The FdA and FdB proteins from *S. metallicus* have very high amino acid identities with respect to both structural templates used (90% for FdA and 83% for FdB) and also have a high amino acid identity (82%) among themselves (see also results). Altogether, this makes us confident that a good structural model can be derived. The program MODELLER (*19*) (version 7) was used for deriving the structures, and the alignments were optimized until a good quality model for the unknown structure was achieved. A Ramachandran analysis of the final models was performed using PROCHECK (*20*). In the final isoform models, the majority of the residues are in the most favored regions (89.3% for FdA and 87.8%), whereas the remaining are found in additional allowed regions.

Molecular Dynamics Simulations. Molecular dynamics simulations were performed using GROMACS (*21*) (version 3.2.1). The GROMOS96 43A1 force field (*22*, *23*), together with the atomic partial charges for the iron sulfur centers, was used as calculated elsewhere (*24*). The simulations started from the comparative model structures (FdA and FdB) using the protonation states at pH 7.0, as determined using previously described methods (*25*, *26*). The system was solvated in a dodecahedral box, where a minimum distance of 8 Å between the protein and the box walls was imposed. The final FdA and FdB systems had 3151 and 2882 water molecules, respectively. The molecular dynamics simulations were performed using separate heat and pressure baths (*27*) at 300 K and 1 bar, respectively, for the solute and solvent (water), coupling constants of 0.1 and 0.5 ps, and an isothermal compressibility of 4.5×10^{-5} bar^{-1}. All bonds were constrained with the LINCS (*28*) algorithm. The equations of motion were integrated using a time step of 2 fs. Nonbonded interactions were treated with a twin-range method, using group-based cutoffs of 8 and 14 Å, updated every 5 steps. The electrostatic forces thus truncated were corrected with a reaction field using a dielectric constant of 54 (*29*), the dielectric constant of SPC water (*30*) under these conditions. The system was energy minimized with the steepest descent method for optimization of the hydrogen atoms. A 10^5 kJ/(mol nm^2) position-restraining force constant on heavy atoms was used in the minimization step. The initialization of each MD simulation was done in two steps. In the first step, a 100 ps simulation was run with all protein heavy atoms position-restrained with a 10^4 kJ/(mol nm^2) force constant and with initial velocities taken from a Maxwellian distribution at 300 K and a temperature and pressure coupling constants of the baths of 0.01 and 0.05 ps, respectively. In the second step, a 100 ps simulation was run with all C^α atoms position-restrained with a 10^4 kJ/(mol nm^2) force constant and temperature and pressure coupling constants of 0.1 and 0.5 ps, respectively. After this initialization, the simulation continued with all atoms free. Conformations were saved every ps for subsequent analysis.

Fluorescence Quenching. Quenching experiments were preformed using acrylamide, a polar nonionic quencher. The samples were excited at 295 nm in order to ensure that the light was absorbed almost exclusively by tryptophanyl groups, and the decrease in maximum fluorescence intensity was analyzed. The results were analyzed according to the Stern−Volmer (eq 1)

$$\frac{F_0}{F} = 1 + K_{SV}[Q] \quad (1)$$

where F_0 and F are the fluorescence intensities in the absence and presence of the quencher, respectively, K_{SV} is the collisional quenching constant, and [Q] is the quencher concentration (*31*). An analysis of the quenching data resulting in negative deviations was carried out using a modification of the Stern−Volmer equation (eq 2)

$$\frac{F}{F_0} = \frac{f_a}{1 + K_{SV}[Q]} + (1 - f_a) \quad (2)$$

which takes into account the fractional contribution of the exposed (f_a) and buried ($1 - f_a$) tryptophans that cause the deviation (*32*).

Thermal Unfolding. Thermal denaturation was followed by monitoring the variation of the spectroscopic signals (Trp emission or Fe−S cluster integrity) as a function of temperature. Typically, 10 μM ferredoxin was used, and a heating rate of 1 °C min^{-1} was used. Data were analyzed according to a two-state model describing how the transition midpoint temperature (T_m) was determined. As with other Fe−S proteins, cluster disintegration is an irreversible process, limiting the thermodynamic analysis to a comparison of the T_m values. As a further control of the thermal transition, we have verified that the Fe−S centers disintegrate at a T_m identical to that determined from Trp intrinsic fluorescence, thus leading to the conclusion that the thermal denaturation of the polypeptide is not influenced by the irreversible character of the denaturation of the Fe−S centers. For the experiments in the presence of different metal chelators, the protein was allowed to incubate for 10 min with chelators (5 mM). This incubation prior to monitoring the thermal transition had no effect on the metal−protein stoichiometry. Curve fitting was carried out using Origin (Microcal).

RESULTS

Ferredoxin Isoform Sequencing and Homology Modeling. Since its original definition, the number of members of the seven iron dicluster ferredoxin family from Archaeal crenarchaeota has been increasing, mostly as a result of genome sequencing projects. The sequences of the two ferredoxin

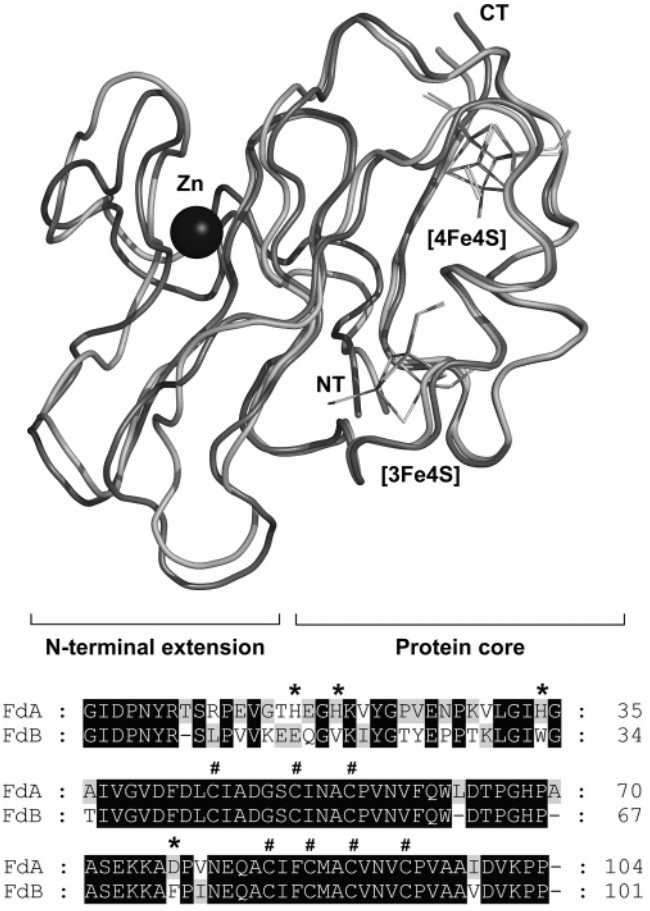

FIGURE 1: Ferredoxin molecular models and amino acid sequences. Top: Structural analysis of ferredoxins FdA (dark gray) and FdB (light gray) built by comparative modeling. The sphere represents the Zn^{2+} center, which is only present in FdA. The proteins are depicted in an orientation that allows the visualization of the *N*-terminal extension (up to residue 35) and the protein Fe−S harboring core. CT, *C*-terminus; NT, *N*-terminus. The Figure was created with PyMOL (*37*). Bottom: Primary sequences of the ferredoxin isoforms. (*), zinc-binding residues; (#), Fe−S cysteine ligands.

isoforms from *S. metallicus* used in this study were determined chemically after proteolytic digestion and sequencing of internal peptides (Figure 1). Both proteins are ∼100 amino acids long and have several of the characteristics of the dicluster ferredoxin family, namely, two iron−sulfur binding Cys motifs (Figure 1, marked with #) and a *N*-terminal extension of ∼30 residues. The two ferredoxin types present within the family differ precisely in this region, and whereas the FdA variants contain a Zn^{2+} binding motif, the FdB isoforms do not (Figure 1, Zn center ligands marked with *). In agreement, the purified ferredoxin isoforms differ in metal content: both contain an ∼6.5 Fe/mol protein, corresponding to the presence of a [3Fe4S] and a [4Fe4S] center, but whereas FdA contains 0.8 Zn/mol protein, the FdB isoform lacks it. Amino acid sequence alignment performed between homologous ferredoxins belonging to this family, confirms their high amino acid identities (79−98%) as noted in the original definition of the family (complete alignment available upon request) (*12*). To correlate ferredoxin conformation and dynamics studies with protein structure, molecular models of the two ferredoxin isoforms were produced by comparative modeling, given the high sequence identity toward members with known structures (see Experimental Procedures for details). Most of the residues differing between the two isoforms under study (20 out of 103) occur at the *N*-terminus (Figure 1).

Stability of Ferredoxin Isoforms Using Molecular Dynamics Simulations. Molecular dynamics (MD) simulations were used to investigate the stability of the ferredoxin isoform structural models, particularly that of the zinc-lacking proteins. Because proteins are very complex systems with multiple minima where the system can easily become trapped during the simulation, the use of a high number of MD-simulation replicates greatly improves the sampling of the system (*33*). Therefore, both FdA and FdB were independently simulated in five molecular dynamics-replicates of 15 ns each. An inspection of the structural models of the two ferredoxins obtained by comparative modeling, which were the starting points for the simulations, evidences an overall identical fold (Figure 1). During the simulation period, both proteins were relatively stable with maximum C^{α} RMSD values of 1.5 and 2.2 Å, respectively, for FdA and FdB (results not shown). Both ferredoxins showed structural changes in the molecular dynamics simulations, and despite the fact that their magnitudes are different, they both occur in the same spatial region. As noted from the analysis of the sequence alignments (Figure 1), the *N*-terminal region of the isoforms is the region in which higher amino acid variability is observed. As a result, this is the part of the proteins in which the larger differences are observed before (Figure 2A and C) and after (Figure 2B and D) the simulations. Although the RMSD of the FdB ferredoxin is a little larger than that of FdA, the RMSD of the region shown in Figure 2 panels B and D is stable (0.15 Å for FdB and 0.10 Å for FdA, within a sphere with a radius of 6 Å from the metal). These computational results are compatible with a stable fold for both isoforms, especially at the *N*-terminal region of the zinc-lacking isoform, and agree well with experimental evidence (see below).

Tryptophan Fluorescence and Quenching. Tryptophan residues are excellent probes for protein conformational changes. FdA has a single tryptophan (Trp62) in a strictly conserved position among the ferredoxin family close to the [3Fe4S] cluster at the protein core. In fact, this residue is also present in FdB (Trp61), and in both cases, they are ca. 40−50% exposed to the solvent, a value that slightly increases after MD simulations in the two ferredoxins but one that nevertheless remains below 50%. The proximity of this common Trp to the Fe−S centers results in fluorescence quenching in the native folded state, and therefore, the fluorescence intensity increases upon Fd unfolding. In addition to this conserved tryptophan, FdB has an additional one (Trp33) in the region bridging the *N*-terminal extension with the protein core. This residue is particularly useful in terms of the analysis of the FdB structure because it occupies the same spatial region in which the Zn^{2+} center is present in the FdA isoforms. Thus, fluorescence quenching was used to probe the conformational dynamics of the two ferredoxins, and acrylamide was used as a quencher in order to probe for differences in Trp accessibility (Figure 3, Table 1). The results obtained show that in FdB a fraction of the Trp moieties is shielded from the solvent, as shown by a negative deviation of the Stern−Volmer curve, which can nevertheless be analyzed using a modified equation that takes into account this effect. This observation is compatible with the contribu-

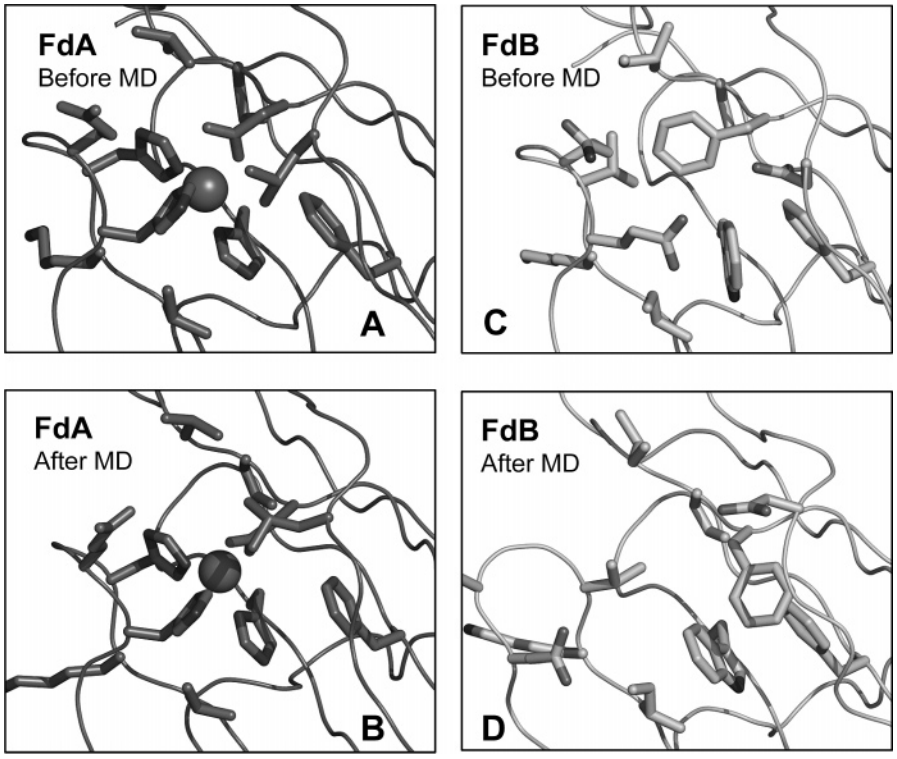

FIGURE 2: Close-up of the FdA zinc region (A and B; dark gray), and the corresponding FdB region (C and D; light gray), showing the structures directly obtained by comparative modeling (A and C) and those obtained by minimization of the MD simulation average (last 12 ns of each MD replicate) (B and D). The protein backbone is represented as a line, zinc as a sphere, and selected residues as sticks. The selected residues are within 6 Å from the zinc in FdA and the corresponding region in FdB. The Figure was created with PyMOL (*37*).

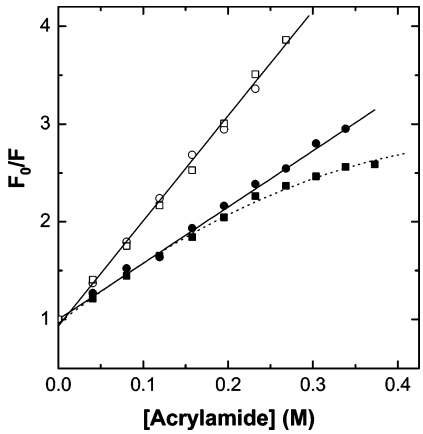

FIGURE 3: Stern−Volmer Plot for tryptophan fluorescence quenching of FdA (○, ●) and FdB (□, ■) either in the native (●, ■) or denatured (○, □) states. The fluorescence measurements were monitored at 345 nm upon excitation at 295 nm. See Table 1 for Stern−Volmer constants.

Table 1: Tryptophan Accessibility Determined from Stern−Volmer Plots

	Stern−Volmer constant K_{sv} (M^{-1})	
protein	FdA	FdB
native	5.8 ± 0.1	6.8 ± 0.5[a]
unfolded	10.2 ± 0.1	10.4 ± 0.2

[a] This K_{sv} value takes into account the fraction of the Trp moieties that are shielded from the solvent. See text for details.

tion arising from the second tryptophan (Trp33) in the *N*-terminal region and shows that this part of the protein has a topology identical to that of the zinc-containing variant. In fact, this observation agrees well with the molecular dynamics studies on FdB. The region around Trp33 remains stable during the MD simulations, and this residue does not get exposed to the solvent during the process. This residue has a very low exposure (∼10%) before and after the MD simulation, even if it increased a little. The environment around Trp 33 in FdB can be inferred by taking the difference between the emission spectra of the two proteins: an emission maximum at 340 nm is observed, which is indicative of a tryptophan moiety predominantly shielded from the solvent (not shown), again an observation that is compatible with the calculated low exposure of this amino acid.

Thermal Stability of Ferredoxin Isoforms. We have investigated the thermal stability of the zinc-containing FdA and zinc-lacking FdB isoforms in a broad pH range between pH 2 and 10. The two ferredoxins are hyperstable proteins. At physiological pH values (pH = 7), these proteins remain folded even upon incubation with high concentrations of denaturants (e.g., 7 M GuHCl or 5 M GuSCN) or at extreme temperatures (up to 100 °C). This observation is in agreement with previous studies on proteins belonging to this family (*12*, *16*, *34*), and it implies that for most thermal unfolding studies some additional destabilization has to be introduced. Ferredoxin unfolding can be evaluated either by monitoring Fe−S cluster decomposition (bleaching of the 410 nm band) or the increase and red shift of the Trp fluorescence maximum (Figure 4). Because of their high stability, the ferredoxins are sufficiently destabilized by extensive protonation to allow unfolding to be observed in the 30−90 °C range only at very acidic pH values (typically below pH 4). In the present study, and in order to study the thermal transition at pH 7 and 10, we had to increase the thermal

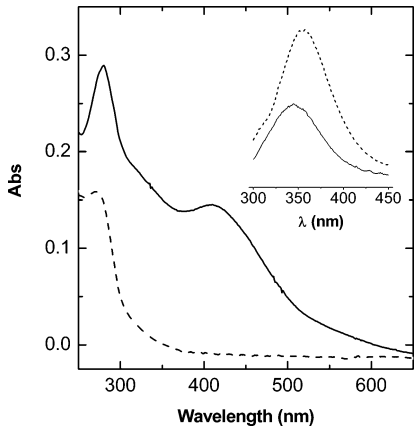

FIGURE 4: Spectroscopic fingerprint of Zn-lacking ferredoxin isoform FdB in the native (—) and denatured (---) states. In the UV−visible spectrum, the band at 410 nm is typical of Fe−S centers and bleaches upon unfolding. The inset shows the emission spectra in arbitrary units upon excitation at 280 nm. Either probe yielded identical results in monitoring thermal transitions.

Table 2: Thermal Midpoint Transitions for Ferredoxins Determined in the Presence of Denaturant at pH 7

[GuHCl] (M)	Fe−S, T_m (°C)		Trp, T_m (°C)	
	FdA	FdB	FdA	FdB
3.0		74.3	69.3	
3.5	61.6		59.0	
4.0	55.0	63.1	55.8	63.5
4.5	49.3	57.1		53.4
5				51.3
5.25				45.6
5.5	36.2	42.6		
0[a]	105.9	113.1	108.6	114.4

[a] Calculated by extrapolation

susceptibility of the ferredoxins by incubating them with different concentrations of GuHCl during thermal unfolding transitions (Table 2). Under these conditions, the thermal transitions were determined for each denaturant concentration used, and the T_m value in water was calculated by performing linear extrapolations (Figure 5, Table 2). For acid pH, the transition midpoints could be determined in the absence of denaturant. The results obtained for the pH dependency study (Table 3) show that the ferredoxin variant lacking the zinc center has consistently higher melting temperatures at all tested conditions and that the stability differences between the two homologous isoforms (ΔT_m) are rather impressive, ranging from 11 to 24 °C. The addition of excess zinc chloride (up to 10 mM) during thermal unfolding has no effect on either isoform.

Effect of Iron and Zinc Chelators on Ferredoxin Thermal Stability. The role of the zinc center in ferredoxin stability was investigated in a series of thermal unfolding experiments that were performed in the presence of different metal chelators. For this study, three different molecules with distinct metal specificities were used: DFO, EDTA, and TPEN. The rationale for this experiment was that by using either iron-specific (DFO, Fe^{3+}), zinc-specific (TPEN, Zn^{2+}), or ambivalent (EDTA) metal chelators we could dissect the relative contribution of the Zn-center with respect to a possible stabilizing role of the iron−sulfur clusters. Thus, if the zinc site has a stabilizing role, the presence of zinc-specific chelators during the thermal unfolding reaction should decrease the T_m because of its scavenging effect. However, if the iron−sulfur clusters would be playing a stabilizing role, then iron-chelating agents should have the same effect. These experiments were carried out at pH 7 and in the presence of 4 M GuHCl to achieve thermal transitions in the working temperature range without the need for extrapolations. The results obtained upon unfolding the two ferredoxins in the presence of different metal chelators are shown in Table 4. It is clear that not one of the chelators has a significant effect over FdB thermal stability, which has an overall constant melting temperature ($T_m = 65 \pm 2$ °C) in all tested conditions. On the contrary, FdA has a significantly lowered stability in the presence of the zinc scavengers TPEN and EDTA ($\Delta T_m = 12°$) but is relatively unaffected by iron chelators. These data suggest that the zinc center plays an important role in stabilizing the isoform that contains it. However, the iron−sulfur centers, which are nevertheless important for the stability of Fe−S proteins (*16*), are not themselves the determinants of the differences in the stabilities of the two ferredoxins studied. In summary, the Zn center is contributing to the enhanced stability of the FdA ferredoxin, but the FdB isoform, which lacks it, has devised a more efficient stabilizing strategy that does not seem to involve a direct contribution from the iron−sulfur centers.

DISCUSSION

Zinc binding sites are very commonly found in proteins as structural elements, as typified by zinc-finger domains. Among the different types of structural zinc centers, the sites from the ferredoxins from thermophilic Sulfolobales constitute a somewhat unique type. In these cases, the metal is tetrahedrally coordinated by His/Asp ligands, and it seems to be involved in maintaining the 3D integrity of a local structural domain comprising an α-helix and three β-strands that constitute the typical *N*-terminal extension found in these proteins. The three imidazole ligands (His 16,19,34 in FdA) are within the β-sheet, whereas the fourth carboxylate ligand (Asp76 in FdA) is distant in the sequence and is located at the surface of the ferredoxin core fold. The latter is characteristic of the super family of [4Fe-4S] ferredoxins (SCOP entry 54862). These zinc centers are unique in iron−sulfur proteins, attaching the *N*-terminal antiparallel β-sheet domain to the $(\beta\alpha\beta)_2$ core. In this respect, this zinc center, which is essentially solvent inaccessible and is involved in the interaction between these two domains of the ferredoxin, combines features of structural and interfacial zinc centers (*3*) because it stabilizes the *N*-terminal domain, promoting its stable interaction with the protein central region. Mutagenesis of the two first histidine ligands (*13*) result in a loss of the zinc center, whereas coordination by aspartic acid was shown to be dispensable (*14*). The removal of the zinc center as well as the truncation of the *N*-terminal extension results in a ferredoxin with decreased thermal stability (*13*, *14*).

The availability of naturally occurring ferredoxin isoforms (*12*) in *S. metallicus* with (FdA) and without (FdB) the zinc center constitutes a powerful tool for studying the contribution of this structural element on ferredoxin fold stability. Here, we have shown that at physiological pH, both FdA and FdB undergo thermal unfolding transitions above the boiling point of water. However, one of the most interesting results was the observation that at all pH values tested (2 <

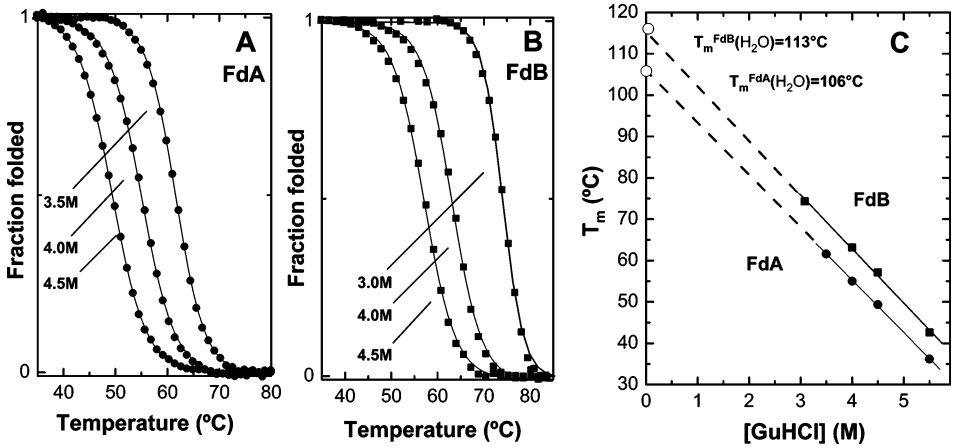

FIGURE 5: Determination of the thermal midpoint transitions in water for ferredoxin isoforms at pH 7. Thermal denaturation is monitored following Fe−S collapse in the presence of different GuHCl concentrations as FdA (panel A) and FdB (panel B) unfold at temperatures above 100 °C. The transition midpoints determined for each denaturant concentrations (Fe−S, T_m in Table 2) are then used to determine the melting temperatures in water ($T_m(H_2O)$), which are obtained by linear extrapolation plots (panel C). Identical results are obtained by monitoring Trp emission variations. Also see Table 2.

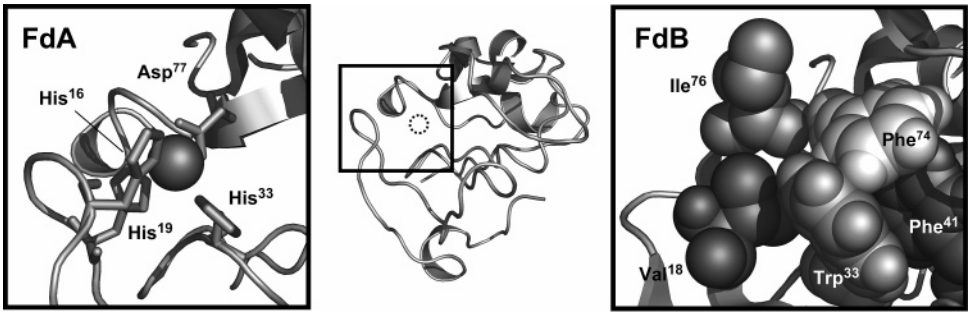

FIGURE 6: Zinc domain coordination in ferredoxin isoforms. The FdA isoforms comprise a set of conserved His/Asp ligands that chelate a structural Zn^{2+} site (A), whereas in FdB, these residues have been replaced by others with higher hydrophobicity (B). The central figure shows the common fold of the proteins and the region that is blown up in the lateral panels. The dotted circle points to the location of the zinc ion in FdA. The Figure was prepared with PyMOL (*37*).

Table 3: Variation of the Thermal Midpoint Transitions in Water for Ferredoxins as a Function of pH

pH	$T_m(H_2O)$ (°C) FdA	$T_m(H_2O)$ (°C) FdB	$\Delta T_m(H_2O)$ (°C)
2	40.5 ± 0.1	64.3 ± 0.1	23.8 ± 0.1
2.5	57.9 ± 0.1	74.9 ± 0.3	17.0 ± 0.3
4	69.2 ± 0.2	82.4 ± 0.4	13.2 ± 0.4
7[a]	105.9 ± 1.1	113.1 ± 2.8	9.2 ± 2.3
10[a]	72.2 ± 3.6	97.0 ± 1.6	24.8 ± 3.9

[a] Calculated by extrapolation as in Figure 5 and Table 2.

Table 4: Effect of Zinc and Iron Chelators on the Ferredoxin Isoform Transition Midpoint Temperatures[a]

	FdA		FdB	
	T_m (°C)	ΔT_m (°C)	T_m (°C)	ΔT_m (°C)
no chelators	55.0		63.1	
DFO	53.3	1.7	65.9	−2.8
TPEN	44.0	11.0	66.9	−3.8
EDTA	43.1	11.9	65.3	−2.2

[a] Conditions: 10 mM Hepes at pH 7, 4 M GuHCl, and 5 mM chelator.

pH < 10) the zinc-lacking isoform (FdB) was always more stable than its zinc-containing counterpart (FdA). This unexpected observation prompted us to investigate the contribution of each metal cofactor to protein stability. For that purpose, we added chelators specific either for zinc (TPEN) or for iron (DFO) during the thermal unfolding transition. What we observed was that these have no effect on the zinc-lacking isoform (FdB) because the measured thermal transition midpoint was basically invariant with respect to the control (T_m = 65 ± 2 °C), showing that the increased stability of this isoform cannot be attributed to a stabilizing effect from the Fe−S centers. However, in the zinc-containing isoform (FdA), zinc chelators (TPEN or EDTA) lead to a decrease in the thermal transition midpoint of ~11 °C, whereas DFO has almost no effect. Thus, we concluded that in ferredoxins containing His/Asp ligands such as FdA, the zinc center contributes to protein stability because its removal results in a less stable protein. However, in the zinc-lacking isoform, the protein fold not only was kept but also was, in fact, more stable. The key question that remains now has to do with what the molecular determinants could be that account for the increased stability of the ferredoxin without the zinc center. An analysis of the structural models at the region where the zinc center is found (Figure 6) shows that the spatial region in which the zinc ligands and the metal would be present is now mostly occupied by hydrophobic residues. This leads to the suggestion that these novel nonpolar interactions arising from this unique spatial arrangement of replacing residues are not only sufficient to stabilize the α-helix/β-sheet *N*-terminal

domain but also result in an enhanced and more efficient stabilization of the zinc domain. It is very interesting to note that a similar strategy has been computationally outlined for stabilizing a zinc-finger domain. Mayo and co-workers have designed, expressed, and determined the structure of a variant peptide (*35*, *36*), which should fold into a $\beta\beta\alpha$ motif based on the backbone structure of a zinc-finger domain. Indeed, the domain was found to be stable without the zinc center, whose removal in zinc-finger proteins results in unfolding (*5*). The computed sequence that resulted in a protein with a $\beta\beta\alpha$ structure comprised two phenylalanines replacing previous zinc-binding ligands that contributed to a well-packed hydrophobic core (*36*). In the case of the proteins used in our study, nature has made a similar design: in FdB, a set of hydrophobic residues (Val18, Phe74, Phe41, Trp33, and Ile76) occupies the spatial region in which the zinc site found is the FdA isoform (Figure 6). This core of hydrophobic residues results in a stabilization of the protein fold, which happens to be more efficient than that provided by metal cross-linking, illustrating the versatility of molecular strategies available to achieve a given 3D structure.

ACKNOWLEDGMENT

We gratefully acknowledge C. Frazão (ITQB) for kindly providing the coordinates of the *A. ambivalens* ferredoxin, J Carita (ITQB Fermentation Service, Oeiras) for cell mass processing, and Professor B. O. Kolbesen and C. Rittmeyer (Johann Wolfgang Goethe-Universität, Frankfurt) for metal analysis by total reflection X-ray fluorescence.

REFERENCES

1. Petsko, G., and Ringe, D. (2004) *Protein Structure and Function*, New Science Press, London, U.K.
2. Hogg, P. J. (2003) Disulfide bonds as switches for protein function, *Trends Biochem. Sci. 28*, 210−214.
3. Auld, D. S. (2001) Zinc coordination sphere in biochemical zinc sites, *Biometals 14*, 271−313.
4. Lee, M. S., Gippert, G. P., Soman, K. V., Case, D. A., and Wright, P. E. (1989) Three-dimensional solution structure of a single zinc finger DNA-binding domain, *Science 245*, 635−637.
5. Lee, M. S., Gottesfeld, J. M., and Wright, P. E. (1991) Zinc is required for folding and binding of a single zinc finger to DNA, *FEBS Lett. 279*, 289−294.
6. Perrier, V., Surewicz, W. K., Glaser, P., Martineau, L., Craescu, C. T., Fabian, H., Mantsch, H. H., Barzu, O., and Gilles, A. M. (1994) Zinc chelation and structural stability of adenylate kinase from *Bacillus subtilis*, *Biochemistry 33*, 9960−9967.
7. Perrier, V., Burlacu-Miron, S., Bourgeois, S., Surewicz, W. K., and Gilles, A. M. (1998) Genetically engineered zinc-chelating adenylate kinase from *Escherichia coli* with enhanced thermal stability, *J. Biol. Chem. 273*, 19097−19101.
8. Green, S. M., Ginsburg, A., Lewis, M. S., and Hensley, P. (1991) Roles of metal ions in the maintenance of the tertiary and quaternary structure of arginase from *Saccharomyces cerevisiae*, *J. Biol. Chem. 266*, 21474−21481.
9. Olry, A., Boschi-Muller, S., Yu, H., Burnel, D., and Branlant, G. (2005) Insights into the role of the metal binding site in methionine-R-sulfoxide reductases B, *Protein Sci. 14*, 2828−2837.
10. Gomes, C. M., Frazao, C., Xavier, A. V., Legall, J., and Teixeira, M. (2002) Functional control of the binuclear metal site in the metallo-beta-lactamase-like fold by subtle amino acid replacements, *Protein Sci. 11*, 707−712.
11. Fujii, T., Hata, Y., Oozeki, M., Moriyama, H., Wakagi, T., Tanaka, N., and Oshima, T. (1997) The crystal structure of zinc-containing ferredoxin from the thermoacidophilic archaeon *Sulfolobus* sp. strain 7, *Biochemistry 36*, 1505−1513.
12. Gomes, C., Faria, A., Carita, J., Mendes, J., Regalla, M., Chicau, P., Huber, H., Stetter, K., and M, T. (1998) Di-cluster, seven-iron ferredoxins from hyperthermophilic Sulfolobales, *J. Biol. Inorg. Chem. 3*, 499−507.
13. Kojoh, K., Matsuzawa, H., and Wakagi, T. (1999) Zinc and an N-terminal extra stretch of the ferredoxin from a thermoacidophilic archaeon stabilize the molecule at high temperature, *Eur. J. Biochem. 264*, 85−91.
14. Kojoh, K., Fukuda, E., Matsuzawa, H., and Wakagi, T. (2002) Zinc-coordination of aspartic acid-76 in Sulfolobus ferredoxin is not required for thermal stability of the molecule, *J. Inorg. Biochem. 89*, 69−73.
15. Leal, S. S., and Gomes, C. M. (2005) Linear three-iron centres are unlikely cluster degradation intermediates during unfolding of iron−sulfur proteins, *Biol. Chem. Hoppe-Seyler 386*, 1295−1300.
16. Leal, S. S., Teixeira, M., and Gomes, C. M. (2004) Studies on the degradation pathway of iron−sulfur centers during unfolding of a hyperstable ferredoxin: cluster dissociation, iron release and protein stability, *J. Biol. Inorg. Chem. 9*, 987−996.
17. Moczygemba, C., Guidry, J., Jones, K. L., Gomes, C. M., Teixeira, M., and Wittung-Stafshede, P. (2001) High stability of a ferredoxin from the hyperthermophilic archaeon *A. ambivalens*: involvement of electrostatic interactions and cofactors, *Protein Sci. 10*, 1539−1548.
18. Stone, K. L., Williams, K. R. (1993) *A Pratical Guide to Protein and Peptide Purification for Microsequencing*, Academic Press, New York.
19. Sali, A., and Blundell, T. L. (1993) Comparative protein modelling by satisfaction of spacial restraints, *J. Mol. Biol. 234*, 779−815.
20. Laskowski, A., MacArthur, M., Moss, D., and Thorton, J. (1993) PROCHECK: a program to check the stereochemical quality of protein structures, *J. Appl. Crystallogr. 26*, 283−291.
21. Lindahl, E., Hess, B., and van der Spoel, D. (2001) GROMACS 3.0: A package for molecular simulation and trajectory analysis, *J. Mol. Model. 7*, 306−317.
22. Scott, W. R. P., Hünenberger, P. H., Tironi, I. G., Mark, A. E., Billeter, S. R., Fennen, J., Torda, A. E., Huber, T., Krüger, P., and van Gunsteren, W. F. (1999) The GROMOS biomolecular simulation program package, *J. Phys. Chem. A 103*, 3596−3607.
23. van Gunsteren, W. F., Billeter, S. R., Eising, A. A., Hunenberger, P. H., Kruger, P., Mark, A. E., Scott, W. R. P., and Tironi, I. G. (1996) *Biomolecular Simulation: The GROMOS96 Manual and User Guide*, BIOMOS b.v., Zurich, Groninger.
24. Teixeira, V. H., Baptista, A. M, Soares, C. M. (2006) Pathways of H2 towards the active site of [NiFe]-hydrogenase, *Biophys. J.* in press.
25. Baptista, A. M., and Soares, C. M. (2001) Some theoretical and computational aspects of the inclusion of proton isomerism in the protonation equilibrium of proteins, *J. Phys. Chem. B 105*, 293−309.
26. Teixeira, V. H., Soares, C. M., and Baptista, A. M. (2002) Studies of the reduction and protonation behavior of the tetraheme cytochromes using atomic detail, *J. Biol. Inorg. Chem. 7*, 200−216.
27. Berendsen, H. J. C., Postma, J. P. M., van Gunsteren, W. F., DiNola, A., and Haak, J. R. (1984) Molecular dynamics with coupling to an external bath, *J. Chem. Phys. 81*, 3684−3690.
28. Hess, B., Bekker, H., Berendsen, H. J. C., and Fraaije, J. G. E. M. (1997) LINCS: A linear constraint solver for molecular dynamics, *J. Comput. Chem. 18*, 1463−1472.
29. Mitou, G., Higgins, C., Wittung-Stafshede, P., Conover, R. C., Smith, A. D., Johnson, M. K., Gaillard, J., Stubna, A., Munck, E., and Meyer, J. (2003) An Isc-type extremely thermostable [2Fe-2S] ferredoxin from *Aquifex aeolicus*. Biochemical, spectroscopic, and unfolding studies, *Biochemistry 42*, 1354−1364.
30. Hermans, J., Berendsen, H. J. C., van Gunsteren, W. F., and Postma, J. P. M. (1984) A consistent empirical potential for water−protein interactions, *Biopolymers 23*, 1513−1518.
31. Lakowicz, J. R. (1999) *Principles of Fluorescence Spectroscopy*, 2nd ed., Kluwer Academic/Plenum Publishers, New York.
32. Chattopadhyay, K., and Frieden, C. (2006) Steady-state and time-resolved fluorescence studies of the intestinal fatty acid binding protein, *Proteins 63*, 327−335.
33. Frazão, C., Silva, G., Gomes, C. M., Matias, P., Coelho, R., Sieker, L., Macedo, S., Liu, M. Y., Oliveira, S., Teixeira, M., Xavier, A. V., Rodrigues-Pousada, C., Carrondo, M. A., and Le Gall, J. (2000) Structure of a dioxygen reduction enzyme from *Desulfovibrio gigas*, *Nat. Struct. Biol. 7*, 1041−1045.

34. Wittung-Stafshede, P., Gomes, C. M., and Teixeira, M. (2000) Stability and folding of the ferredoxin from the hyperthermophilic archaeon *Acidianus ambivalens*, *J. Inorg. Biochem. 78*, 35−41.
35. Dahiyat, B. I., Sarisky, C. A., and Mayo, S. L. (1997) De novo protein design: towards fully automated sequence selection, *J. Mol. Biol. 273*, 789−796.
36. Dahiyat, B. I., and Mayo, S. L. (1997) De novo protein design: fully automated sequence selection, *Science 278*, 82−87.
37. DeLano, W. L. (2002) *The PyMOL User's Manual*, DeLano Scientific, San Carlos, CA.

BI0610698